Journal of Biomedical Optics

BiomedicalOptics.SPIEDigitalLibrary.org

Laser speckle imaging based on photothermally driven convection

Caitlin Regan
Bernard Choi

SPIE.

Journal of Biomedical Optics 21(2), 026011 (February 2016)

Laser speckle imaging based on photothermally driven convection

Caitlin Regan[a,b] **and Bernard Choi**[a,b,c,d,e,*]
[a]University of California–Irvine, Department of Biomedical Engineering, 3120 Natural Sciences II, Irvine, California 92697, United States
[b]Beckman Laser Institute and Medical Clinic, 1002 Health Sciences Road East, Irvine, California 92612, United States
[c]University of California–Irvine, Department of Surgery, 333 City Boulevard West, Suite 1600, Orange, California 92868, United States
[d]Edwards Lifesciences Center for Advanced Cardiovascular Technology, 2400 Engineering Hall, Irvine, California 92697, United States
[e]CHOC Children's Hospital, 1201 West La Veta Avenue, Orange, California 92868, United States

Abstract. Laser speckle imaging (LSI) is an interferometric technique that provides information about the relative speed of moving scatterers in a sample. Photothermal LSI overcomes limitations in depth resolution faced by conventional LSI by incorporating an excitation pulse to target absorption by hemoglobin within the vascular network. Here we present results from experiments designed to determine the mechanism by which photothermal LSI decreases speckle contrast. We measured the impact of mechanical properties on speckle contrast, as well as the spatiotemporal temperature dynamics and bulk convective motion occurring during photothermal LSI. Our collective data strongly support the hypothesis that photothermal LSI achieves a transient reduction in speckle contrast due to bulk motion associated with thermally driven convection. The ability of photothermal LSI to image structures below a scattering medium may have important preclinical and clinical applications.
 [DOI: 10.1117/1.JBO.21.2.026011]

Keywords: laser speckle imaging; blood; photothermal; convection; expansion; mechanism.

Paper 150777R received Nov. 17, 2015; accepted for publication Jan. 25, 2016; published online Feb. 26, 2016.

1 Introduction

Laser speckle imaging (LSI) is an interferometric technique that provides information about the motion of optical scatterers in a sample.[1–10] Fercher and Briers first applied LSI to visualize blood vessels in the retina.[1] Researchers have since reported on the use of LSI to map blood flow in many organs, including the brain,[5,6] skin,[7–9] and kidneys.[10]

Conventional LSI has limited ability to quantify blood flow and resolve vasculature below a static scattering layer such as the epidermis or skull. Speckle contrast values measured with LSI are associated with contributions from photons interacting with both static and dynamic scatterers.[2] Contributions from overlying static scatterers to the detected speckle pattern reduce the dynamic range of LSI and the overall visibility of subsurface microvasculature.[11,12]

To overcome this limitation, we previously reported on the method of photothermal LSI.[13] With the application of a 3 ms pulse of 595 nm laser light, we observed a transient increase in the visibility of a subsurface microchannel containing flowing blood and of subsurface blood vessels in a mouse dorsal window chamber model. In Ref. 13, we postulated that selective photothermal excitation of hemoglobin molecules in the red blood cells resulted in an increase in the motion of scattering particles within the vessels, leading to a simultaneous transient reduction in speckle contrast and hence increased visibility of subsurface microvasculature. This was based, in part, on published reports of photothermal optical coherence tomography,[14] photoacoustic imaging,[15] pulsed photothermal radiometry,[16] and photothermal spectroscopy.[17]

Here we describe experiments designed to identify the primary mechanism by which photothermal LSI decreases speckle contrast. We proposed the following three hypotheses:

1. A thermally induced pressure wave, similar to the photoacoustic effect, induces a bulk increase in motion throughout the sample.
2. An increase in temperature induces local effects such as changes in optical properties, viscosity of blood, Brownian motion, protein denaturation, and formation of methemoglobin.[18,19]
3. Thermally driven convection, a bulk movement of the liquid due to temperature gradients generated by the photothermal excitation, results in the motion of the irradiated medium.

For hypothesis 1, we compared the photothermal excitation pulse duration τ_p (3 ms) with the characteristic stress relaxation time of the sample τ_s. For efficient pressure-wave generation to occur, τ_p should be significantly shorter than $\tau_s = \delta/c_s$, where δ is the absorption length and c_s is the speed of sound in the medium.[20] For blood with 100% oxygen saturation, $\delta \sim 0.03$ mm at 595 nm excitation[21] and $c_s = 1.48 \times 10^6$ mm/s,[22] resulting in τ_s of 20 ns. Hence, as $\tau_p \gg \tau_s$, we rejected hypothesis 1 as a primary mechanism. In this work, we present results from experiments designed to test hypotheses 2 and 3.

*Address all correspondence to: Bernard Choi, E-mail: choib@uci.edu

1083-3668/2016/$25.00 © 2016 SPIE

2 Materials and Methods

2.1 *Liquid and Solid Phantoms*

Our liquid phantom consisted of 0.8 mL of rabbit whole blood (~18°C) placed in a 35 mm diameter Petri dish, resulting in a layer thickness of 0.83 mm. We also used a solid silicone phantom (35 mm diameter, 10 mm thick) fabricated using a polydimethylsiloxane (PDMS) base, with TiO_2 powder added to provide scattering and India ink to provide absorption.[23]

2.2 *Photothermal Laser Speckle Imaging Setup and Data Analysis*

Our LSI setup [Fig. 1(a)] consisted of a HotShot 1280 CCD camera (NAC Image Technology, Simi Valley, California) fitted with a macro lens. We used an exposure time of 9 ms and a frame rate of 100 fps. The speckle imaging laser was a diffused, long-coherence (~6 m) 808 nm laser diode (Ondax, Monrovia, California), and the photothermal excitation laser was a 595 nm pulsed dye laser (Vbeam, Candela, Wayland, Massachusetts) emitting a 3 ms pulse (10 mm diameter) at a radiant exposure of 4 J/cm^2.

To study speckle contrast dynamics outside the directly irradiated spot, we increased the imaging field of view to extend laterally 12.5 mm beyond the spot. We collected image sequences spanning the time before, during, and after the excitation pulse. We converted each raw speckle image to a spatial speckle contrast image using a conventional 7×7 sliding window algorithm.[2] We calculated the average speckle contrast of each image in a region of interest (ROI) selected within the directly irradiated spot (black) and ~10 mm away from the edge of the irradiated spot (red) [Fig. 2(a)].

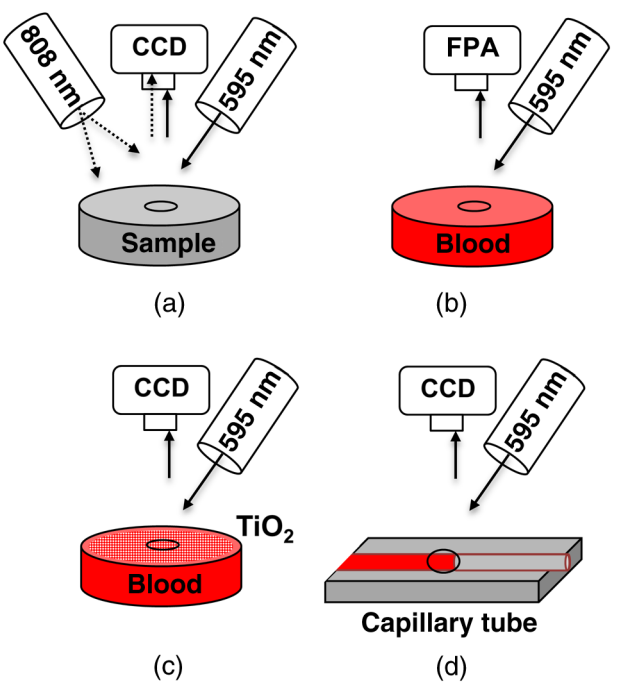

Fig. 1 (a) Photothermal LSI setup. We performed LSI on blood and solid silicone phantoms with a CCD camera and an 808 nm laser. We used a 595 nm pulsed laser to excite the 10 mm region indicated at the center of each sample. (b) A midinfrared focal plane array (FPA) was used to detect infrared emission generated in blood as a result of a 595 nm photothermal excitation pulse. (c) A CCD camera was used to acquire high-speed images of the radial movement of TiO_2 particles on the surface of a blood sample during the 595 nm photothermal excitation pulse. (d) A CCD camera was used to visualize the expansion of blood in a microcapillary tube upon irradiation by the 595 nm pulsed laser.

2.3 *Infrared Thermal Imaging*

To study heat diffusion dynamics, we used a midinfrared focal plane array (FLIR Systems, Wilsonville, Oregon) to collect images of the whole blood phantom described above, at 271 fps and with a 0.8 ms exposure time per frame [Fig. 1(b)]. We collected images over a period of 5 s during photothermal excitation and used a blackbody source (OMEGA Engineering, Stamford, Connecticut) to convert the infrared emission images to calibrated radiometric temperature maps.

2.4 *Particle Image Velocimetry*

To study convection dynamics, we distributed particles of TiO_2 powder on the surface of a layer of whole blood contained in a Petri dish. We collected high-speed (800 fps) brightfield images of the entire blood sample [Figs. 1(c) and 4(a)] over a period of 87.5 ms during photothermal excitation. We used particle image velocimetry (PIV) methodology[24] to map vectors associated with the motion of the TiO_2 particles and processed the data using MatPIV software[24] developed in MATLAB® (The Mathworks, Natick, Massachusetts).

2.5 *Volume Expansion in a Capillary Tube*

We infused whole blood into a 650-μm diameter glass microchannel embedded at the surface of a scattering PDMS phantom (reduced scattering coefficient $\mu_s' \sim 1\ mm^{-1}$) [Fig. 1(d)]. We collected both raw speckle images and brightfield images of the phantom during photothermal excitation. We calculated speckle contrast versus time in three ROIs within the microchannel [Fig. 4(c)].

3 Results and Discussion

3.1 *Photothermal Laser Speckle Imaging of Liquid and Solid Phantoms*

To assess the degree of correlation between local temperature and local speckle contrast, we measured speckle contrast during photothermal LSI in both the region directly irradiated by the pulsed laser and in a surrounding nonirradiated region ~10 mm away [Figs. 1(a) and 2]. Figure 2(a) shows speckle contrast versus time, with photothermal excitation beginning at time = 0 s. The contrast in each ROI was the same before the pulse. Immediately after the onset of pulsed laser excitation, the contrast values in both ROIs decreased simultaneously, suggesting a similar change in motion occurring throughout the entire sample, not just in the irradiated spot. We did not observe bubble formation or cavitation in the blood at this radiant exposure.

We performed a similar experiment on a solid silicone phantom to determine how the mechanical properties of the sample affect the photothermal LSI response. When the excitation pulse was applied to the solid phantom, the contrast decreased

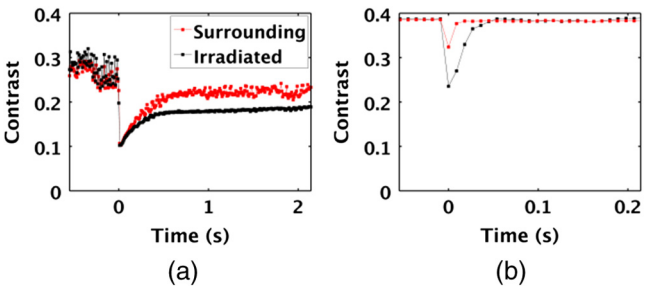

Fig. 2 Photothermal excitation induces changes in speckle contrast in both the directly irradiated and the surrounding regions of a sample. The dynamics of speckle contrast may depend on the mechanical properties of the sample. (a) Immediately following excitation of a 0.83 mm thick layer of blood with the pulsed dye laser, speckle contrast within and 10 mm away from the laser spot decreased, suggesting that photothermal excitation causes effects throughout the entire sample. (b) Speckle contrast dynamics during the 0.2 s immediately following photothermal excitation of a solid tissue-simulating phantom; contrast decreased and recovered ~10× more quickly than the irradiated blood sample in (a).

immediately and simultaneously in both ROIs [Fig. 2(b)], similar to our observations with the photothermal excitation of blood [Fig. 2(a)]. However, the contrast in the surrounding region only decreased to ~40% of the change measured in the directly irradiated spot. Due to the higher stiffness of silicone, the contrast throughout the solid phantom returned to its baseline value within ~50 ms, which is 10 times faster than the associated recovery time for blood [Fig. 2(a)].

Collectively, these data (Fig. 2) suggest that photothermal excitation induces motion throughout the entire sample, and not just in the directly irradiated spot, and that the dynamics of this motion are affected by the mechanical properties of the sample [i.e., compare Figs. 2(a) and 2(b)].

3.2 *Thermal Response to Photothermal Excitation*

We next measured the spatiotemporal temperature dynamics in response to photothermal excitation of blood [Figs. 1(b) and 3]. With photothermal excitation [beginning at time = 0 s in Fig. 3(a)], we observed an instantaneous increase in radiometric temperature of ~50°C in the directly irradiated spot. The temperature rise caused by the excitation pulse was localized to the directly irradiated region [Fig. 3(b)]. Following the rapid increase in radiometric temperature, we observed a relatively slow decrease toward room temperature.

After 4.4 s, the peak temperature decreased by ~78%, but the elevated temperature remained confined primarily to the directly irradiated spot. The temperature in the region surrounding this spot changed minimally during the 5 s imaging duration [Fig. 3(b)]. These data demonstrate that the temperature increased appreciably only in the directly irradiated site.

Our data demonstrate that photothermal excitation of whole blood induces changes in speckle contrast throughout the entire sample that recover to near-baseline values in <1 s (Fig. 2), whereas temperature changes over the same period of time are restricted only to the directly irradiated spot (Fig. 3). These results strongly suggest that local changes alone cannot explain the relatively widespread decrease in speckle contrast observed with photothermal LSI. Hence, based on our findings, we rejected hypothesis 2 as a primary mechanism.

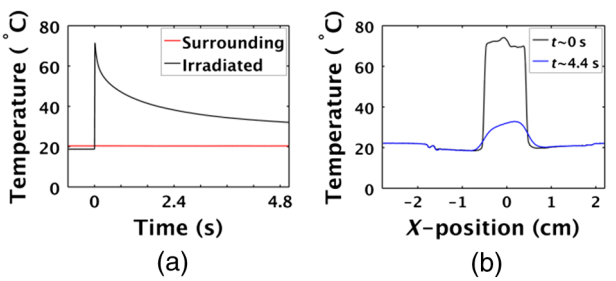

Fig. 3 Photothermal excitation induces a change in temperature that is localized to the directly irradiated region. (a) With pulsed dye laser excitation of a layer of blood, the radiometric temperature increased ~50°C, followed by a relatively slow decay over a period of seconds. Outside the directly excited region, the temperature did not appreciably change. (b) Line profile of radiometric temperature immediately following the excitation pulse (black) and ~4.4 s following the pulse (blue). The temperature rise caused by the excitation pulse is localized to the irradiated region and remained laterally confined to the diameter of the laser pulse throughout the measurement period (~4.4 s).

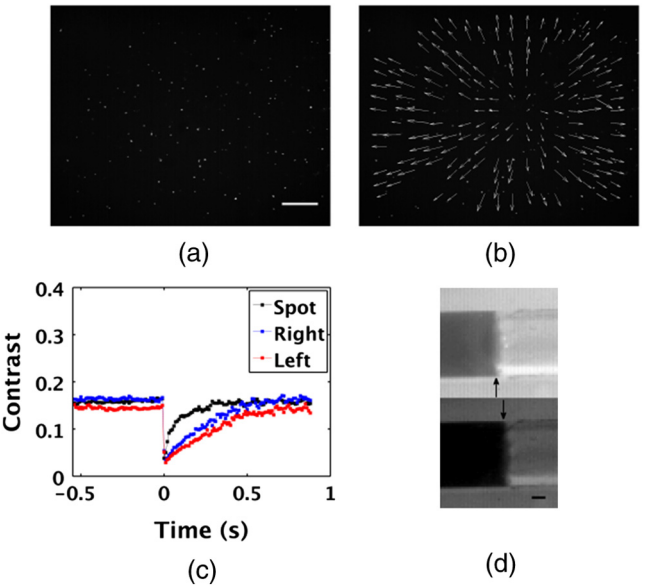

Fig. 4 Following pulsed laser excitation, bulk motion of blood occurs due to thermally driven volume expansion. (a) Brightfield image of a 2 mm thick layer of blood (scale bar = 1 mm) with TiO_2 particles suspended on the surface. The accompanying video shows the lateral displacement of the particles following the excitation pulse (Video 1, MP4, 0.3 MB) [URL: http://dx.doi.org/10.1117/1.JBO.21.2.026011.1]. (b) PIV image showing the vector field associated with particle displacement. The vectors demonstrate that the motion in the sample radiates outward from the center of the excitation pulse. (c) Speckle contrast versus time of blood in a glass capillary tube. Contrast is shown for ROIs both inside the irradiated region (black) and in regions adjacent to the directly irradiated region. When the photothermal excitation pulse is applied (time = 0 s), the contrast immediately drops in all three regions, not just the irradiated spot. (d) Brightfield image of blood (dark) in a capillary tube before (above) and immediately after (below) photothermal excitation (scale bar = 100 μm) showing the expansion that occurred. We postulate that the decrease in intensity in the lower frame is associated with saturation of the CCD sensor during photothermal excitation, as in subsequent frames there is no change in intensity of the blood or background.

3.3 *Thermally Driven Convective Motion (Volume Expansion)*

We next used suspended TiO_2 particles [Figs. 1(c), 4(a), and 4(b)] to test hypothesis 3: thermally driven convection induced by photothermal excitation leads to bulk motion of blood away from the directly irradiated spot, causing an increase in motion throughout the entire sample. Convective motion is a bulk flow of fluid due to both diffusive and advective transport. In our experiments, we believe the driving force is the temperature difference between the irradiated region and the surroundings. In particular, the Marangoni effect causes convective motion of liquids due to gradients in surface tension.[25] The surface tension of the heated blood is lower than that of the surroundings,[26] providing a driving force for the liquid to move outward from the irradiated region. We imaged over a period of 87.5 ms during photothermal excitation. Immediately following the excitation pulse, we observed a rapid bulk motion of the particles away from the irradiated spot throughout the entire imaging field of view [Fig. 4(a), Video 1)].

We used PIV concepts[24] to map vectors associated with the motion of the TiO_2 particles between the initial frame and the frame in which the particles are in their final displaced position. The map of the velocity field of the particles [Fig. 4(b)] illustrates the bulk motion of the TiO_2 particles away from the center of the directly irradiated spot.

To determine whether this bulk motion also occurs in a vessel-like structure, we next performed photothermal LSI and brightfield imaging on whole blood inside a glass capillary tube [Figs. 1(d), 4(c), and 4(d)]. With photothermal LSI, we observed an instantaneous decrease in contrast within the irradiated region (black), as well as the regions to the right (blue) and left (red) of the laser pulse, with subsequent recovery to baseline values [Fig. 4(c)]. With brightfield images of the blood–air interface, we observed immediate motion of blood to $\sim 70\ \mu m$ beyond the initial position after photothermal excitation.

The 4 J/cm^2 radiant exposure of the photothermal excitation pulse that we used in this study is above the ANSI safety limit of 0.26 J/cm^2 for skin.[27] To investigate this further, we performed preliminary calculations with a Monte Carlo layered model to investigate the fluence distribution $\Phi(z)$ and maximum temperature rise expected in human skin. With use of thermal properties from a previous publication, we estimated the maximum temperature rise (assuming no heat diffusion during the pulse) $\Delta T = \Phi(z)\mu_a(z)/(\rho c)$ in the epidermis[28] to be 42°C. Although the calculated epidermal temperature rise is high, published clinical data using pulsed laser excitation at 577 and 585 nm of both normal and port-wine stain skin demonstrate that higher radiant exposures (>6.5 J/cm^2) can be used without any observable epidermal injury.[29,30] Further research is warranted to investigate the sensitivity and safety of photothermal LSI to radiant exposure and to different sets of optical properties.

In conclusion, our collective data (Figs. 2–4) strongly support hypothesis 3—that photothermal LSI achieves a transient reduction in speckle contrast due to bulk motion associated with thermally driven convection, and is not due to pressure wave generation (hypothesis 1) or local effects driven by temperature dynamics (hypothesis 2).

Due to the relative simplicity of photothermal LSI, further work is warranted to study its potential applications for fluid characterization, biological, and biomedical research. In this and our previous work,[13] we focused on photothermal excitation of hemoglobin; we postulate that this approach can be extended to excitation of other endogenous and exogenous chromophores. The ability of photothermal LSI to image structures below a scattering medium may have important preclinical and clinical applications in future studies of theranostic contrast agent development, epithelial cancer, and angiogenesis.

Acknowledgments

The authors would like to acknowledge support from the Arnold and Mabel Beckman Foundation, the Air Force Office of Scientific Research (FA9550-14-1-0034), the National Institutes of Health (R01 DE022831, R01 HD065536), the National Institutes of Health Laser Microbeam and Medical Program (P41 EB015890), and the National Science Foundation BEST IGERT Program (DGE 1144901).

References

1. A. F. Fercher and J. D. Briers, "Flow visualization by means of single-exposure speckle photography," *Opt. Commun.* **37**, 326–330 (1981).
2. D. A. Boas and A. K. Dunn, "Laser speckle contrast imaging in biomedical optics," *J. Biomed. Opt.* **15**, 011109 (2010).
3. B. Choi, N. M. Kang, and J. S. Nelson, "Laser speckle imaging for monitoring blood flow dynamics in the in vivo rodent dorsal skin fold model," *Microvasc. Res.* **68**, 143–146 (2004).
4. A. J. Moy et al., "Wide-field functional imaging of blood flow and hemoglobin oxygen saturation in the rodent dorsal window chamber," *Microvasc. Res.* **82**, 199–209 (2011).
5. A. K. Dunn et al., "Dynamic imaging of cerebral blood flow using laser speckle," *J. Cereb. Blood Flow Metab.* **21**, 195–201 (2001).
6. P. C. Li et al., "Imaging cerebral blood flow through the intact rat skull with temporal laser speckle imaging," *Opt. Lett.* **31**, 1824–1826 (2006).
7. S. Sharif et al., "Noninvasive clinical assessment of port-wine stain birthmarks using current and future optical imaging technology: a review," *Br. J. Dermatol.* **167**, 1215–1223 (2012).
8. Y. C. Huang et al., "Blood flow dynamics after laser therapy of port wine stain birthmarks," *Laser Surg. Med.* **41**, 563–571 (2009).
9. Y. C. Huang et al., "Noninvasive blood flow imaging for real-time feedback during laser therapy of port wine stain birthmarks," *Laser Surg. Med.* **40**, 167–173 (2008).
10. C. Sturesson et al., "Laser speckle contrast imaging for assessment of liver microcirculation," *Microvasc. Res.* **87**, 34–40 (2013).
11. A. B. Parthasarathy et al., "Robust flow measurement with multi-exposure speckle imaging," *Opt. Express* **16**, 1975–1989 (2008).
12. J. C. Ramirez-San-Juan et al., "Spatial versus temporal laser speckle contrast analyses in the presence of static optical scatterers," *J. Biomed. Opt.* **19**, 106009 (2014).
13. C. Regan, J. C. Ramirez-San-Juan, and B. Choi, "Photothermal laser speckle imaging," *Opt. Lett.* **39**, 5006–5009 (2014).
14. D. C. Adler et al., "Photothermal detection of gold nanoparticles using phase-sensitive optical coherence tomography," *Opt. Express* **16**, 4376–4393 (2008).
15. X. Wang et al., "Noninvasive laser-induced photoacoustic tomography for structural and functional in vivo imaging of the brain," *Nat. Biotechnol.* **21**, 803–806 (2003).
16. B. C. Li et al., "Accurate measurement of blood vessel depth in port wine stained human skin in vivo using pulsed photothermal radiometry," *J. Biomed. Opt.* **9**, 961–966 (2004).
17. G. H. Brilmyer et al., "Photothermal spectroscopy," *Anal. Chem.* **49**, 2057–2062 (1977).
18. A. M. K. Nilsson et al., "Changes in optical properties of human whole blood in vitro due to slow heating," *Photochem. Photobiol.* **65**, 366–373 (1997).
19. L. L. Randeberg, A. J. Daae Hagen, and L. O. Svaasand, "Optical properties of human blood as a function of temperature," *Proc. SPIE* **4609**, 20–28 (2002).
20. L. V. Wang, *Biomedical Optics: Principles and Imaging*, Wiley, Hoboken, New Jersey (2007).

21. S. A. Prahl, "Tabulated molar extinction coefficient for hemoglobin in water," 4 March 1998, http://omlc.ogi.edu/spectra/hemoglobin/summary.html (April 2014).
22. P. A. Hasgall et al., "IT'IS database for thermal and electromagnetic parameters of biological tissues," Version 2.4, 30 July 2013, www.itis.ethz.ch/database (April 2014).
23. F. Ayers et al., "Fabrication and characterization of silicone-based tissue phantoms with tunable optical properties in the visible and near infrared domain," *Proc. SPIE* **6870**, 687007 (2008).
24. J. K. Sveen and J. Kolaas, "An introduction to MatPIV v.1.7," 15 April 2014, http://www.mn.uio.no/math/english/people/aca/jks/matpiv/ (August 2014).
25. J. M. Drezet and S. Mokadem, "Marangoni convection and fragmentation in laser treatment," *Mater. Sci. Forum* **508**, 257–262 (2006).
26. J. Rosina et al., "Temperature dependence of blood surface tension," *Physiol. Res.* **56**(Suppl. 1), S93–S98 (2007).
27. Northwestern University Office for Research Safety, "Laser safety handbook," 2011, http://www.research.northwestern.edu/ors/forms/laser-safety-handbook.pdf (January 2016).
28. B. Choi and A. J. Welch, "Analysis of thermal relaxation during laser irradiation of tissue," *Laser Surg. Med.* **29**, 351–359 (2001).
29. J. S. Nelson et al., "Dynamic epidermal cooling in conjunction with laser-induced photothermolysis of port wine stain blood vessels," *Laser Surg. Med.* **19**, 224–229 (1996).
30. O. T. Tan, K. Sherwood, and B. A. Gilchrest, "Treatment of children with port-wine stains using the flashlamp-pulsed tunable dye-laser," *New Engl. J. Med.* **320**, 416–421 (1989).

Caitlin Regan is a PhD candidate in biomedical engineering at University of California, Irvine. She received her BS degree in bioengineering (mechanics) from California Institute of Technology.

Bernard Choi is currently an associate professor in the Departments of Biomedical Engineering and Surgery at the University of California, Irvine, with appointments in the Beckman Laser Institute and the Edwards Lifescience Center for Advanced Cardiovascular Technology. He received his PhD in biomedical engineering from the University of Texas at Austin.